Fermi National Accelerator Laboratory

FERMILAB-Pub-92/147-A
May 1992

LARGE-SCALE MICROWAVE ANISOTROPY FROM GRAVITATING SEEDS[1]

SHOBA VEERARAGHAVAN◇ AND ALBERT STEBBINS♣

◇ Physics & Astronomy Department, University of Massachusetts[2]

♣ NASA/Fermilab Astrophysics Center[3]

Subject Headings: cosmology: theory - cosmic microwave background

ABSTRACT. Topological defects could have seeded primordial inhomogeneities in cosmological matter. We examine the horizon-scale matter and geometry perturbations generated by such seeds in an expanding homogeneous and isotropic universe. Evolving particle horizons generally lead to perturbations around motionless seeds, even when there are compensating initial underdensities in the matter. We describe the pattern of the resulting large-angular scale microwave anisotropy. Anisotropies generated by moving seeds on horizon scales are likely to be significant.

It is generally believed that structure in the universe has developed by gravitational instability from small primordial inhomogeneities in matter. In one class of models, the matter inhomogeneities develop around topologically stable defects such as cosmic strings or domain walls which are generated in a cosmological phase transition[1,2], around short-lived 'knots' of cosmic texture[3], or around scalar field condensates such as soft bosons[4]. Since their gravitational fields are typically quite weak, the seeds are 'stiff' in that their evolution is negligibly affected by the gravitational inhomogeneities they produce. In an earlier paper[5], we developed the linear theory of the growth of inhomogeneities and metric disturbances in a cosmology containing stiff matter seeds. We paid particular attention to seeds produced in a initially homogeneous universe, in which case the seeds are always compensated by inhomogeneities in the matter.

Here, we calculate the linear gravitational fields in specific models of seeds, with and without compensating initial matter underdensities (because the observable consequences can be very different). Although our seed configurations are simplistic, more realistic configurations can only be handled numerically, and would not illustrate as nicely the essential phenomenology in seed cosmologies. We also calculate the Sachs-Wolfe microwave temperature anisotropy, which is the most important observable effect of very large-scale

[1] Shortened version to appear in *The Astrophysical Journal Letters*

[2] Amherst, MA 01003

[3] MS209, FNAL, Box 500, Batavia, IL 60510-0500

inhomogeneities. The anisotropies considered here are quite different from the small-scale anisotropies previously considered for cosmic strings[6-9], collapsing texture knots[10], or collapsing domain wall bags[11], all of which are generated by the motions of the seeds. We find that even static seeds can generate anisotropies because information about their existence travels outward at the finite speed of light, thus the gravitational fields are not static at the causal horizon. Secondly, the small angular scale anisotropies were calculated for a static vacuum background, while our seeds are surrounded by cosmological matter whose distribution is perturbed by the seeds, thus generating further microwave distortions which may add to or cancel the total anisotropy. These are absent in the vacuum case.

II. Gravitational Fields of a Point Mass, a String, and a Wall

We take the speed of light, c, and Newton's constant, G, to be unity unless specified otherwise. We assume a flat Friedmann-Robertson Walker (FRW) cosmology containing on average a critical density of dust, thus the matter is cold, dark, and dissipationless (CDM). The metric, including perturbations due to the seeds is, to first order,

$$g_{mn}(\mathbf{x},\eta) = a^2\,\mathrm{diag}\,[-1,1,1,1] + a^2\,h_{mn}(\mathbf{x},\eta), \qquad a(\eta) \propto \eta^2, \tag{2.1}$$

where η and $\mathbf{x}$ are conformal time and comoving position, respectively, and a is the scale factor. We use the synchronous gauge with $h_{oo} = h_{oi} = 0$.

If the seeds were created from an initially homogeneous universe, then conservation of energy and momentum mandates that the energy and the momentum of the seed be compensated by perturbations in the energy and momentum of the matter fields, *i.e.* the CDM, within the same horizon volume (VS §3e[5]). If the seeds were created at some very early time when the horizon was very small, the detailed spatial distribution of the initial compensation does not matter on larger "macroscopic" scales. If we distribute the initial matter and velocity compensations "locally", that is, so that the growing mode density perturbation is everywhere proportional to the source energy density, we obtain solutions for the CDM density and background metric which remain self-similar. If the universe is not initially homogeneous, or the apparent initial horizon is much smaller than the true horizon due to an early inflationary phase, the seeds may not be compensated by initial matter inhomogeneities on the scale of the horizon, but instead there may be metric perturbations so that the gravitational field equations are satisfied. We then obtain another set of self-similar gravitational fields.

Once the initial conditions are chosen, the CDM density perturbation δ_c evolves according to,

$$\ddot{\delta}_c + \frac{2}{\eta}\dot{\delta}_c - \frac{6}{\eta^2}\delta_c = 4\pi(\Theta_{oo} + \Theta_{ii}), \tag{2.2}$$

where Θ_{mn} is the stress-energy tensor of the seed. Taking the limit $\eta_i \to 0$ avoids introducing a scale in the problem, because the density evolves to a pure growing mode, $\delta_c \propto \eta^2$, while η is still arbitrarily small.

Of course, our universe has not always been dust-dominated. The comoving horizon size at the time of equal densities in CDM and radiation, η_{eq}, introduces a new scale. In the radiation era, part of the compensation resides in the radiation. Sound waves and free-streaming of the radiation smooth this compensation exponentially over a scale of order η_{eq} (VS[5]). Since this scale is accessible to cosmological large-scale structure observations and microwave anisotropy measurements, corrections due to the radiation may be significant. However, since we consider only very large-scale effects, we can ignore the radiation corrections.

1. A Point Mass

The simplest type of seed is a localized concentration of energy. If this point mass seed remains stationary, its net stresses are zero, and its gravitational fields are identical to those of CDM. Thus, compensating the point mass with CDM results in an essentially perfectly homogeneous universe.

On the other hand, an initially uncompensated point mass is equivalent to a point overdensity in the CDM. This is a well-studied example, but it is nevertheless instructive. The total mass accreted around the point mass grows with the scale factor and soon dominates the initial seed. Let the point mass be at the centre of the coordinate system, and let the total mass of the overdensity (assumed much bigger than the seed mass M_*), grow at late times as $M(\eta) = \eta^2 M_0$. Normalising so that $\eta_\circ = a(\eta_\circ) = 1$ today, there is a CDM point overdensity of magnitude $2\pi M(\eta)/3$. From the formulae in VS[5], we see that the metric disturbances extend beyond the particle horizon,

$$h_{ij} = \frac{M(\eta)}{|\mathbf{x}|^3}\left(\frac{x^i x^j}{|\mathbf{x}|^2} - \frac{1}{3}\delta_{ij}\right)\left(1 + 5\frac{|\mathbf{x}|^2}{\eta^2}\right) \qquad |\mathbf{x}| > 0. \tag{2.3}$$

Thus uncompensated seeds are acausal in the sense that they require adjustment of the metric at points which have not been in causal contact with the seed ($|\mathbf{x}| > \eta$). Notice that equation (2.3) does not make the usual Newtonian assumption that the scale of spatial gradients is much smaller than the horizon scale ($\nabla^{-1} \ll \eta$), hence it generalises the usual form of the Newtonian metric for a point mass[12].

2. Infinite Straight Cosmic String

In certain theories with a symmetry breaking phase transition, a scalar field is trapped along topologically stable linelike regions of positive energy density. This is a cosmic string[13]. We represent the stress-energy of a static cosmic string along the z axis as $\Theta_{mn}(\mathbf{x},\eta) = \mu\,\mathrm{diag}[1,0,0,-1]\,\delta(x)\,\delta(y)$ where $G\mu/c^2$ is the dimensionless rest-frame mass per unit length. Since the width of a Grand Unified cosmic strings is only a few hundred Planck lengths, the stress-energy distribution of a string in its transverse is well approximated by a δ-function. Although the energy perturbation very close to a string is highly nonlinear, the gravitational fields of the string are weak[1] and linear theory provides

a good approximation for the metric perturbations. There is no net gravitational force on the CDM around the string (eqn 2.2).

First consider an uncompensated cosmic string. Vilenkin[1] showed that the static spacetime around a string in vacuum is flat with a conical singularity at the string. The spatial manifold transverse to the string is a 2-dimensional cone with an angular deficit $8\pi\mu$. To construct a flat FRW cosmology with an uncompensated string, we multiply the vacuum metric by a time dependent conformal factor a^2, where $a(\eta)$ is just the FRW scale factor[13,14]. Since the two metrics are conformally related, the FRW spatial slices have the same conical geometry as do the vacuum spatial slices. There are no initial matter inhomogeneities and none can develop. It would be difficult to detect such a string because the spacetime is locally flat (except on the string) and the matter fields are completely uniform. An observer within the horizon of the string can detect it via gravitational lensing, but outside its horizon there is no detectable effect.

Next, consider the compensated string. If the string is created from an initially homogeneous universe, there must be a compensating underdensity in the matter, which at late times is, $\delta_c = -2\pi\mu\eta^2\delta(x)\delta(y)/5$. The metric perturbation has rotational symmetry about the string axis,

$$h_{ij}(\mathbf{x},\eta) = \mu\Upsilon_1(u)\begin{bmatrix}1 & 0 & 0\\ 0 & 1 & 0\\ 0 & 0 & -2\end{bmatrix} + \mu\Upsilon_2(u)\begin{bmatrix}\cos 2\psi & \sin 2\psi & 0\\ \sin 2\psi & -\cos 2\psi & 0\\ 0 & 0 & 0\end{bmatrix} + \frac{2\mu}{5}\frac{\delta(u)}{u}\begin{bmatrix}1 & 0 & 0\\ 0 & 1 & 0\\ 0 & 0 & 0\end{bmatrix}, \tag{2.4}$$

where $x = r\cos\psi$, $y = r\sin\psi$, $u \equiv r/\eta$, and for $0 < u \leq 1$,

$$\Upsilon_1(u) = 2\left[\ln\left(\frac{1+\sqrt{1-u^2}}{u}\right) - \frac{1}{3}(1-u^2)^{\frac{3}{2}} - \sqrt{1-u^2}\right], \qquad \Upsilon_2(u) = -\frac{2}{5}\frac{(1-u^2)^{\frac{5}{2}}}{u^2}. \tag{2.5}$$

This result can be obtained from the equations of VS[5]. For a different approach see ref. 15. A nonzero, evolving, gravitational field around a compensated static string might initially appear surprising. However, since there is no conservation law constraining the string tension (equivalently, Θ_{ij}), it is *not* compensated in the initial conditions. Thus the stresses give rise to nonzero fields in regions in causal contact with the string. Outside the horizon, the metric functions of course vanish smoothly. As the horizon evolves outward at the speed of light, the metric also evolves. Since the string introduces no new length scale, h_{ij} evolves self-similarly, depending only on the ratio $u = r/\eta$ of the comoving distance from the string to the comoving horizon.

The gravitational field of the string alone (ignoring the compensating initial matter underdensity) is tracefree with amplitude $\frac{4}{3}\Upsilon_1$ in our gauge. Thus the other terms in equation (2.4) are due to the linelike compensating underdensity. Very close to the string the metric becomes singular, with $\Upsilon_1 \to -2\ln(u)$ and $\Upsilon_2 \to -2/5u^2$, apart from the

δ-function. The logarithmic divergence is due to the conical singularity at the assumed infinitely thin string. This term becomes smooth and finite upon modeling the finite width of a gauge string[13]. The other divergences are the linearized, synchronous gauge representation of the gravitational field of a line of underdensity, which creates a $\frac{1}{r}$ repulsive force. On small scales, radiative free-streaming and non-linear clustering of the CDM smooth out the divergent underdensity over a finite region with finite underdensity.

3. Infinite Flat Domain Wall

When the topologically stable positive energy density regions of the scalar field are sheetlike, a domain wall results. The energy-momentum tensor for a static domain along the $x-y$ plane in a matter-dominated flat FRW cosmology is $\Theta_{mn} = a(\eta)\sigma\delta(z)\mathrm{diag}[1,-1,-1,0]$, where σ is the mass per unit area of the wall. This stress-energy tensor approaches zero sufficiently quickly as $\eta_i \to 0$ that the initial compensation is effectively zero. Thus there is no distinction between an initially uncompensated wall and a compensated wall. Using the formulae in VS[5], the linear metric perturbation is

$$h_{ij} = \frac{4\pi}{7} a\sigma\eta^2\delta(z)\,\mathrm{diag}\,[0,0,1]\,. \tag{2.6}$$

This metric is nonzero only at the wall itself. The wall in its neighbourhood stretches out the synchronous coordinates in the transverse direction, hence repelling the CDM. This repulsion evacuates a region of physical thickness $\frac{4\pi}{7}(a\eta)^2\sigma$ resulting in a CDM underdensity,

$$\delta_c = -\frac{2\pi\sigma}{7} a(\eta)\eta^2\delta(z). \tag{2.7}$$

The wall generates its own compensation even in an initially uniform universe, but this underdensity remains localised in the neighbourhood of the wall. It is *not* expelled elsewhere, because there are no tidal forces, and everywhere else the CDM density remains uniform. This does not mean that particle number conservation is violated, because the underdensity arises from stretching the evacuated volume at the wall.

III. Microwave Temperature Patterns

We now consider perturbations of the temperature of an initially uniform gas of photons due to the time-variation of the gravitational fields[16]. This Sachs-Wolfe effect manifests itself as an angular variation in the microwave temperature pattern around the observer,

$$\frac{\Delta T_{\mathrm{SW}}}{T}(\hat{\mathbf{n}}) = -\frac{1}{2}\int_{\eta_{ls}}^{\eta_o} \hat{n}^i\,\hat{n}^j\,\dot{h}_{ij}(\mathbf{x}_\gamma(\eta),\eta)\,d\eta \tag{3.1}$$

where $\mathbf{x}_\gamma(\eta) = (\eta_o - \eta)\hat{\mathbf{n}}$ describes the photon trajectory along the line of sight $\hat{\mathbf{n}}$, η_{ls} is the conformal time at which the photons were last scattered, and η_o is the conformal time of observation. We typically assume that $\eta_{ls} = 0$ except where doing so would lead

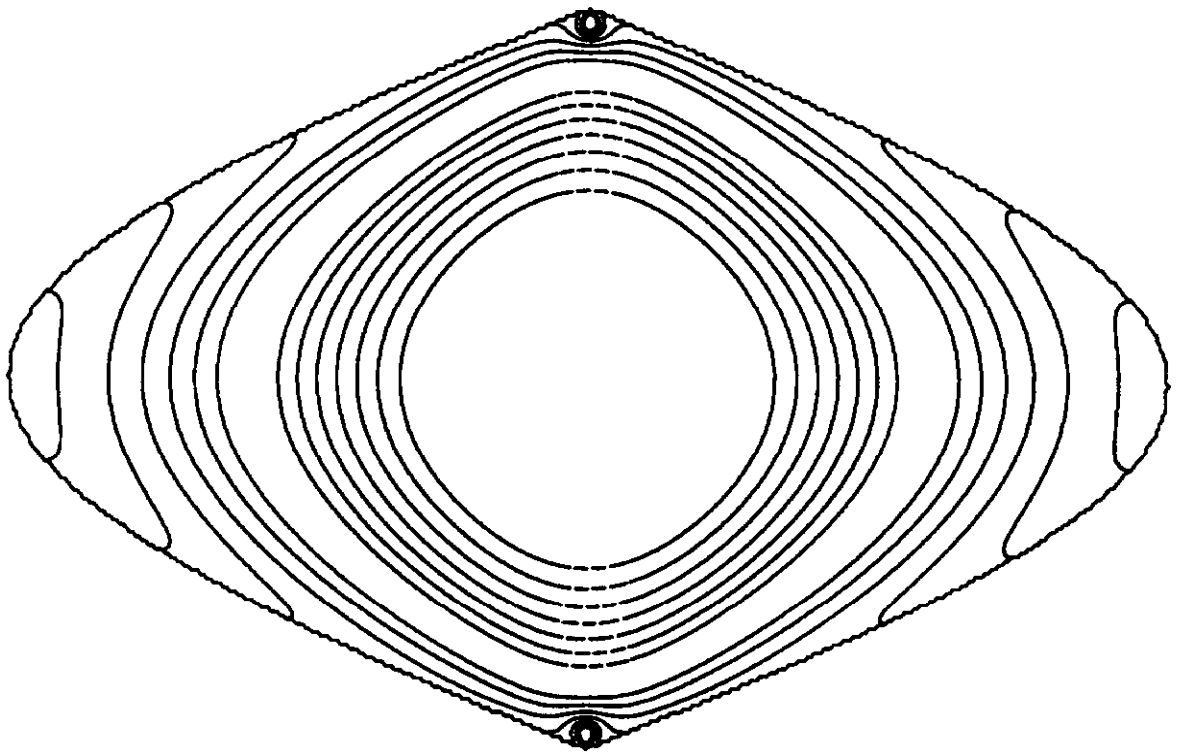

Figure 1 : An all-sky map, centred on the observer, of the temperature anisotropy pattern with monopole subtracted, for a single string at closest redshift 0.13 (fractional distance $u_o = 0.06$). The string lies parallel to the polar axis. The contour limits are $\pm 5\mu$, and the contour spacing is 0.714μ. The solid contours are positive-valued, the dashed contours are negative-valued. The dipole is most prominent, and there are two hotspots at the string "endpoints" which mark the angular extent of string inside the observer's horizon.

to an unphysical divergence, and also assume that the matter-era solutions of §II are adequate. Averaging equation (3.1) over all photon directions and all volume gives the *mean* anisotropy,

$$\overline{\frac{\Delta T_{\rm SW}}{T}} = \frac{1}{3}\left[\overline{\delta}_{\rm c}(\eta_o) - \overline{\delta}_{\rm c}(\eta_{\rm ls})\right] . \tag{3.2}$$

That is, the average microwave temperature decreases faster (slower) than in a pure matter-dominated universe if the seeds result in a net decrease (increase) in the average CDM overdensity, $\overline{\delta}_{\rm c}$. Although a mean temperature is not measurable, this argument suggests that we would see a hotspot (coldspot) when looking towards an isolated seed which has created a local overdensity (underdensity). The compensated point mass and the uncompensated string do not change $\overline{\delta}_{\rm c}$, so no anisotropy is expected. The compensated string and the wall generate growing underdensities and hence a net reddening of photons. In general, a compensated seed produces a net blue (red)-shift if its average equation of state satisfies $p\,(\text{pressure}) > -\frac{1}{3}\rho\,(\text{density})$ ($p < -\frac{1}{3}\rho$) while an uncompensated seed produces a net blue (red)-shift if p/ρ for the seed is greater (less) than that for

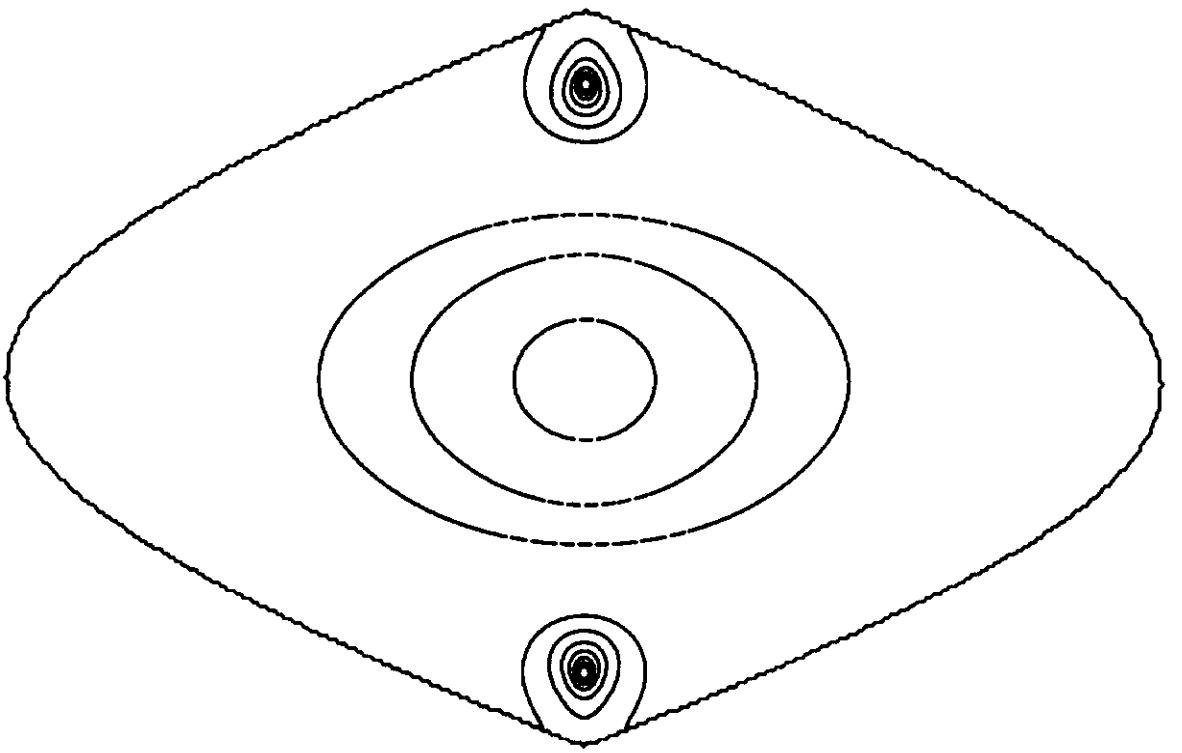

Figure 2 Same as Figure 1 for a string at redshift 1 ($u_o = 0.30$). The dipole is less prominent though it still dominates. The bluespots are more clearly visible though of lower amplitude.

the matter background.

In a flat matter-dominated universe with pure growing mode perturbations, the peculiar gravitational potential, Φ, at a fixed comoving point does not change with time and (3.1) yields the classical result[12,16] that the anisotropy comprises a gravitational redshift term and a Doppler term due to the peculiar velocity difference between observer and last scattering:

$$\frac{\Delta T_{\rm SW}}{T} = \frac{1}{3}[\Phi(\mathbf{x}_\gamma(\eta_{\rm ls})) - \Phi(\mathbf{x}_\gamma(\eta_o))] + \frac{1}{3}[\eta_{\rm ls}\hat{\mathbf{n}}\cdot\nabla\Phi(\mathbf{x}_\gamma(\eta_{\rm ls})) - \eta_o\hat{\mathbf{n}}\cdot\nabla\Phi(\mathbf{x}_\gamma(\eta_o))]. \quad (3.3)$$

Note that even if the gravitational fields are strong near the seeds or compensation, the anisotropies need not be large. Physically, this is because photons which gain energy falling into a deep potential well lose this energy climbing out. There is a net energy change only if they are emitted deep within the well. Also, the anisotropy pattern can extend over the entire sky, unless the gravitational fields are localised.

1. The Pattern from a Point Mass

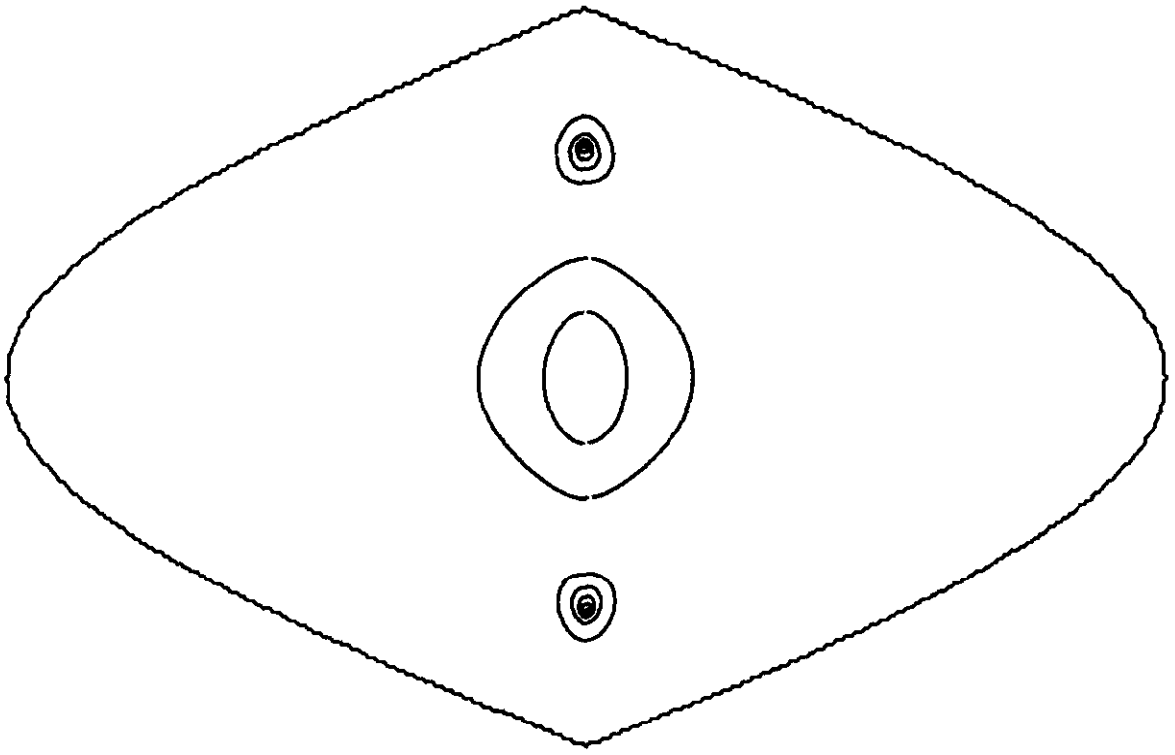

Figure 3 Same as Figure 1 for a string at redshift 3.7 ($u_o = 0.54$). [contour plot: redshift 3.0, $u_o = 0.50$] The two hotspots are still visible, the dipole amplitude is greatly reduced, and a cold strip begins to show up parallel to the string.

The temperature around a compensated mass is uniform and we will not consider it further. The pattern around an uncompensated mass is circularly symmetric,

$$\frac{\Delta T_{\rm SW}}{T}(\hat{\mathbf{n}}) = \frac{1}{3}\left[\frac{M\eta\hat{\mathbf{n}}\cdot\mathbf{x}_\gamma}{a|\mathbf{x}_\gamma|^3} + \frac{M}{a|\mathbf{x}_\gamma|}\right]_{\eta=0}^{\eta_o}. \tag{3.4}$$

Since the gravitational field of an uncompensated point mass is equivalent to that of a purely scalar growing mode, we could have also obtained this result by substituting the potential, $\Phi = -M/a|\mathbf{x}|$, into Eq. (3.3).

2. The Pattern from a Single String

The metric around an uncompensated string is static, and hence produces no Sachs-Wolfe anisotropy. In contrast, the compensated string produces a characteristic linelike pattern. Only a finite length of such a string lies within the observer's horizon, and only this length affects the anisotropy. Although different points on the string are at different distances from the observer, the location of the string can be characterised by the comoving distance u_o to its closest point ($0 < u_o \leq 1$, normalised so that $u_o = 1$ is at the observer's horizon today), and every other point is at a greater distance from the observer.

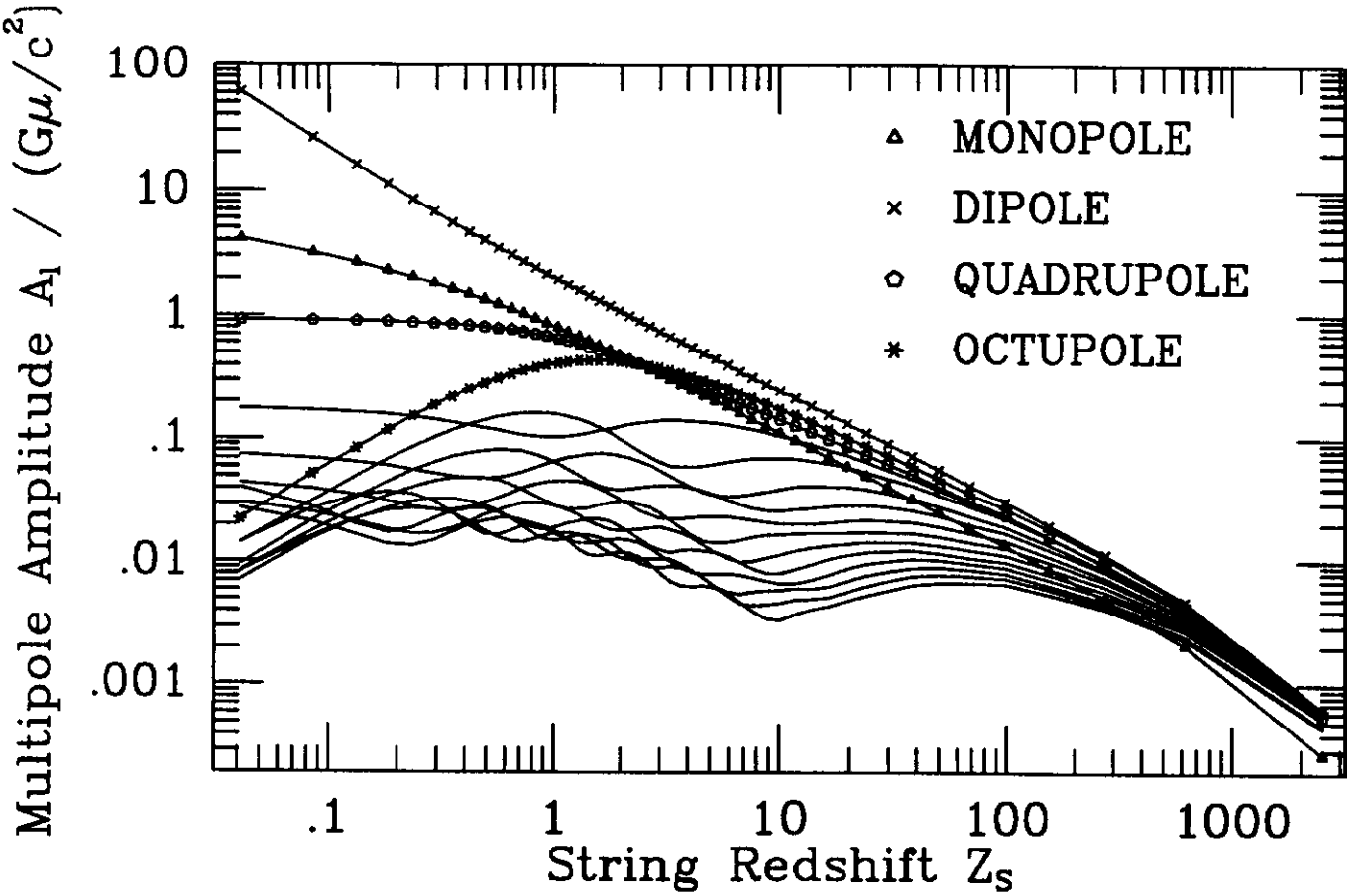

Figure 4 Multipole amplitudes A_l, for the anisotropy pattern around a single string, as a function of the closest redshift for strings at varying distances from oberver. The lowest four moments are identified. A_l is defined so that $< |\Delta T_{SW}/T|^2 >= \sum_{l=0}^{\infty}(2l+1)|A_l|^2$.

In Figures 1-3, we show all-sky maps of the anisotropy (the unobservable monopole term is subtracted) on a latitude-longitude grid, for strings at redshifts 0.13, 1.0, 3.0 (comoving distances $u_o = 0.06, 0.30, 0.50$). The maps are oriented so that the string lies parallel to the polar axis at zero longitude, and its nearest point lies along zero latitude. The anisotropy is calculated numerically. For strings at high redshift, the pattern is a red strip along the string with a width equal to the apparent horizon size at the string redshift, and with hotspots at the two "endpoints" of the string (the points at highest redshift) which are in the deepest part of the potential well. The anisotropy is small in other directions. For string at lower redshifts, the anisotropy pattern grows in size and a dipole pattern arises as the observer is repelled away from the compensation around the string. Figure 4 shows the multipole amplitudes for the lowest 16 multipoles (including the unobservable monopole and dipole) as a function of string redshift. At low redshifts, the dipole and lower order multipoles dominate, but as the redshift increases, higher multipoles begin to dominate.

To understand the figures better, consider the temperature at certain points where the Sachs-Wolfe integral is analytical. At the endpoint hotspots the potential only grows

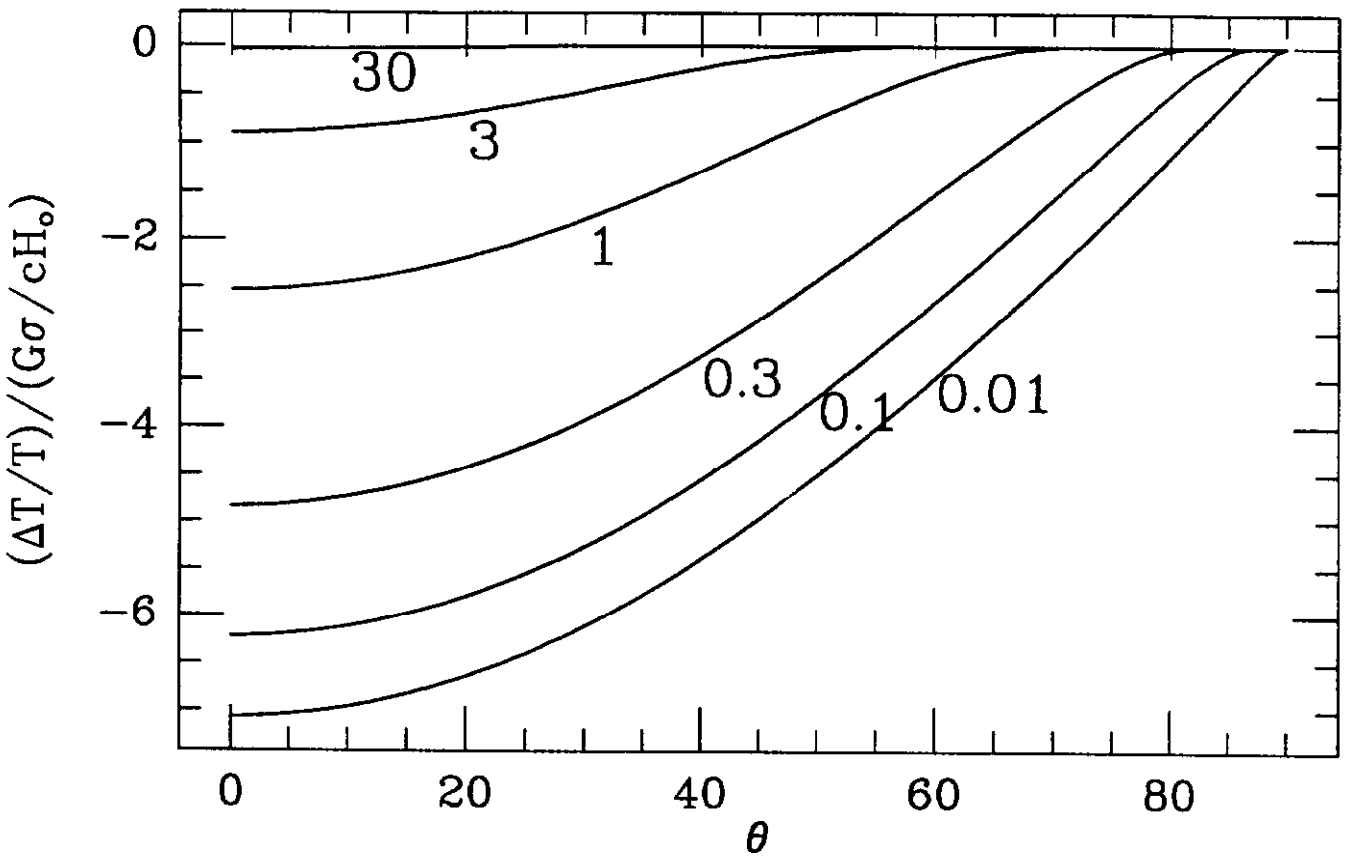

Figure 5 Profile of temperature fluctuations observed as a function of angular distance from the centre of a domain wall, for walls at varying distances from the observer. The numbers identify the closest redshift of the wall. The all-sky temperature pattern is circularly symmetric.

logarithmically, hence

$$\frac{\Delta T_{\rm SW}}{T} = \frac{12}{5}\mu\,(1-u_{\rm o}^2)^{\frac{5}{2}}\ln\left|\frac{\eta_{\rm o}}{\eta_{\rm ls}}\right|, \tag{3.5}$$

which is bounded by the finite time of last scattering: $\Delta T/T \leq 8.3\mu$. In the limit that the string approaches the observer ($u_{\rm o} \to 0$), the two endpoints approach the poles. At the poles, the anisotropy equals $\mu\Upsilon_1(u_{\rm o})$, however the apparent logarithmic divergence for small $u_{\rm o}$ is in fact truncated to approach the limiting value above. Note that classical Sachs-Wolfe theory predicts *zero* anisotropy at the poles because they lie along surfaces of constant Newtonian potential whose gradient is perpendicular to the line of sight! In the direction opposite the string,

$$\frac{\Delta T_{\rm SW}}{T} = \frac{\mu}{5}\left[2\ln\frac{u_{\rm o}}{1+\sqrt{1-u_{\rm o}^2}} - 3\cos^{-1}u_{\rm o}\right] + 2\sqrt{1-{u_{\rm o}}^2}\left[1+\frac{u_{\rm o}}{2}+\frac{1}{u_{\rm o}}+\frac{2}{3}(1-{u_{\rm o}}^2)^{3/2}\right]. \tag{3.6}$$

The temperature diverges as $\frac{2}{5}\mu({u_{\rm o}}^{-1}+\ln u_{\rm o})$ as the string approaches the observer ($u_{\rm o} \to 0$), due to the Sachs-Wolfe Doppler and potential terms from the compensating line of

underdensity. The underdensity repels the observer, leading to blueshifted photons, but the observer is also high up in a potential well, which redshifts the photons.

3. The Pattern from a Wall

Since the field of a wall is localised, only photons which pass through the wall would suffer a temperature change. Consider a domain wall at a comoving distance r_o from the observer. Only a finite circular region of the wall centred around the closest point on the wall lies within the horizon of the observer. Thus the observer sees a circular pattern of anisotropy. The temperature pattern is uniform outside a radius θ_w given by,

$$\cos\theta_w = \frac{r_o}{\eta_o}. \tag{3.7}$$

A photon moving at an angle θ to the perpendicular to the wall which passes through the wall at time η_w experiences a temperature jump equal to $-8\pi a(\eta_w)\sigma\eta_w\cos\theta/7$ which grows with η_w. To understand this, note that the comoving frames in which photon energy is measured are accelerated away from the repulsive wall in opposite directions. In the frame of the observer, this translates to a Doppler redshift as the photon crosses the wall. The velocity difference between the two frames, $\frac{8\pi}{7}a\sigma\eta$ is just twice the velocity generated by a static wall[17].

A photon coming from an angle θ passes through the wall at time $\eta_w = \eta_o - r_o/\cos\theta$. If z_w is the redshift of the wall centre, the observed temperature pattern is,

$$\begin{aligned}\frac{\Delta T_{SW}}{T} &= -\frac{16\pi\sigma}{7H_0}\cos\theta\left(1-\frac{\cos\theta_w}{\cos\theta}\right)^3 \\ &= -\frac{16\pi\sigma}{7}\cos\theta_w\left[1-\frac{1-(1+z_w)^{-1/2}}{\cos\theta}\right]^3, \qquad \theta<\theta_w\equiv 1-(1+z_w)^{-1/2}.\end{aligned} \tag{3.8}$$

which goes smoothly to zero at the edge of the circle. Figure 5 demonstrates how both the size and maximum temperature deviation of the spot decrease as the redshift of the wall increases.

IV. Implications

Even the simplest and most quiescent configurations of topological defects can produce observable effects in the form of density perturbations, differential flows of matter, and MBR anisotropy. For an uncompensated accreting point mass, anisotropies and flows extend beyond its horizon. For a compensated point mass, all observable effects are suppressed. However, it is not generally true that compensation suppresses observable effects of the defects. The compensated string has flows and anisotropies that extend to, but not beyond, its horizon. The uncompensated string, whose gravitational field consists only

of an angular deficit, does not generate flows or anisotropies, but has altered the global properties of the spacetime since its angular deficit extends beyond its horizon. However, an observer not in causal contact with the string cannot observe it, while a causally connected observer has only the gravitational lensing probe. Thus the compensated string is easier to observe. In the case of walls, both the compensated and uncompensated wall are equally observable.

It is usually assumed that only moving seeds can generate anisotropies. In fact, cosmological effects can produce anisotropies even around static seeds, and compensation is not in general sufficient to remove these anisotropies. Upon comparing numbers, we see that the amplitude of anisotropy due to cosmological horizons is comparable or smaller than the anisotropy due to motions in a vacuum background: the typical anisotropy when looking directly at a single moving vacuum string is roughly $4\pi\mu^{6-8}$, which is somewhat larger than the 8.3μ at the hotspots of a nearby compensated static FRW string. For domain walls, it has been calculated[11] that the anisotropy from a spherical wall bubble collapsing at redshift z_w and with a maximal size equal to the horizon at collapse, is about $8\pi\mathcal{A}\sigma/3H_0(1+z_w)^{3/2}$ ($\mathcal{A} \leq 19$), whereas the maximal anisotropy from a static FRW wall at the same redshift is down by a factor $6/(7\mathcal{A})$. The patterns extend over comparable scales. Since in most models, a realistic configuration contains more than one defect per horizon, our calculated anisotropies are a lower bound to the large-scale observable anisotropy in those models. Most defects are mildly relativistic, hence including motion would further increase the anisotropies to the values found in small-angular-scale calculations with moving string networks[9], but on somewhat larger scales (Veeraraghavan & Stebbins 1991, in preparation).

Acknowledgments: This work was supported in part by the NSF at Amherst and by the DOE and the NASA (grant # NAGW-2381) at Fermilab

References

1. A. Vilenkin, *Gravitational field of vacuum domain walls and strings*, *Phys. Rev.* **D23** (1981), 852-857.

2. C. Hill, D. Schramm, and J. Fry, *Cosmological Structure Formation from Soft Topological Defects*, *Comm. Nucl. Part. Physics* **19** (1989), 25-39.

3. N. Turok, *Global Texture as the Origin of the Large Scale Structure of the Universe*, *Phys. Rev. Lett.* **63** (1989), 2625-2638.

4. W. Press, B. Ryden, and D. Spergel, *Single Mechanism fo Generating Large Scale Structure and Providing Dark Missing Matter*, *Phys. Rev. Lett.* **64** (1990), p. 1084-1087.

5. S. Veeraraghavan and A. Stebbins [VS], *Causal Compensated Perturbations in Cosmology*, *Astrophys. J.* **365** (1990), 37-65.

6. N. Kaiser and A. Stebbins, *Microwave Anisotropy due to Cosmic Strings*, *Nature* **310** (1984), 391-393.

7. R. Gott, *Gravitational Lensing Effects of Vacuum Strings: Exact Solutions*, *Astrophys. J.* **288** (1985), 422-427.

8. A. Stebbins, *Cosmic Strings and the Microwave Sky I: Anisotropy from Moving Strings*, *Astrophys. J.* **327** (1988), 584-614.

9. F. Bouchet, D. Bennett, and A. Stebbins, *Patterns of the cosmic microwave background from evolving string networks*, *Nature* **335** (1988), 410-414.

10. N. Turok and D. Spergel, *Global Texture and the Microwave Background*, *Phys. Rev. Lett.* **64** (1990), 2736-2739.

11. M. Turner, R. Watkins, and L. Widrow, *Microwave Distortions form Collapsing Domain-Wall Bubbles*, *Astrophys. J. Lett.* **367** (1991), L43-L47.

12. J. Peebles, §§84 & §§93, "*The Large Scale Structrure of the Universe*", Princeton University Press, Princeton, 1980.

13. A. Vilenkin, *Cosmic Strings and Domain Walls*, *Physics Reports* **121** (1985), 263-315.

14. R. Gregory, *Cosmological Cosmic Strings*, *Phys. Rev. D* **39** (1989), 2108-2114.

15. J. Magueijo, *Giving Cosmic Strings a Birthday*, DAMTP preprint.

16. R. Sachs and A. Wolfe, *Perturbations of a Cosmological Model and Angular Variations of the Microwave Background*, *Astrophys. J.* **147** (1967), 73-90.

17. A. Stebbins and M. Turner, *Is the Great Attractor Really a Great Wall?*, *Astrophys. J. Lett.* **339** (1989), L13-L16.